Parameters influencing the deposition of methylammonium lead halide iodide in hole conductor free perovskite-based solar cells

Bat-El Cohen, Shany Gamliel, and Lioz Etgar

Citation: APL Materials **2**, 081502 (2014); doi: 10.1063/1.4885548
View online: http://dx.doi.org/10.1063/1.4885548
View Table of Contents: http://scitation.aip.org/content/aip/journal/aplmater/2/8?ver=pdfcov
Published by the AIP Publishing

APL MATERIALS **2**, 081502 (2014)

Parameters influencing the deposition of methylammonium lead halide iodide in hole conductor free perovskite-based solar cells

Bat-El Cohen, Shany Gamliel, and Lioz Etgar[a]
Institute of Chemistry, Casali Center for Applied Chemistry, The Hebrew University of Jerusalem, Jerusalem 90400, Israel

(Received 16 May 2014; accepted 17 June 2014; published online 25 June 2014)

Perovskite is a promising light harvester for use in photovoltaic solar cells. In recent years, the power conversion efficiency of perovskite solar cells has been dramatically increased, making them a competitive source of renewable energy. An important parameter when designing high efficiency perovskite-based solar cells is the perovskite deposition, which must be performed to create complete coverage and optimal film thickness. This paper describes an in-depth study on two-step deposition, separating the perovskite deposition into two precursors. The effects of spin velocity, annealing temperature, dipping time, and methylammonium iodide concentration on the photovoltaic performance are studied. Observations include that current density is affected by changing the spin velocity, while the fill factor changes mainly due to the dipping time and methylammonium iodide concentration. Interestingly, the open circuit voltage is almost unaffected by these parameters. Hole conductor free perovskite solar cells are used in this work, in order to minimize other possible effects. This study provides better understanding and control over the perovskite deposition through highly efficient, low-cost perovskite-based solar cells. [http://dx.doi.org/10.1063/1.4885548]

In recent years, organo-metal perovskite has been used as a light harvester in solar cells. The high efficiency perovskite-based solar cells are simple to fabricate and low cost, making them a competitive source of renewable energy.[1,2] Kojima *et al.* were the first to use solution-processed methylammonium (MA) lead halide iodide ($CH_3NH_3PbI_3$) perovskite as a sensitizer on mesostructured TiO_2 using a liquid electrolyte, achieving a power conversion efficiency (PCE) of 3.8%.[3] However, these cells suffered from major stability issues. The use of solid hole conductor material in $CH_3NH_3PbI_3$ perovskite solar cells demonstrated a PCE of 9.7%[4] with much better stability. Recently PCEs of more than 16% were demonstrated for perovskite-based solar cells.[5,6]

Substitution of the iodide with chloride achieved $MAPbI_{(3-x)}Cl_x$ perovskites, which were deposited on mesoscopic TiO_2 and Al_2O_3 achieving PCEs of 7.6% and 10.9%, respectively.[7] One of the attractive properties of the perovskites is their ability to act both as light harvester and hole conductor with a low exciton binding energy, making the fabrication of solar cells based on these perovskites much simpler compared to organic photovoltaic (OPVs) or dye-sensitized solar cells (DSSCs).[8,9] Moreover, the structure of perovskite solar cells is not restricted to mesoporous structure, and efficient planar perovskite solar cells have been demonstrated as well.[10,11]

Several deposition techniques are used for perovskite-based solar cells, including vapor deposition, vapor assisted solution process (VASP), and solution processed via one-step and two-step deposition.[12–14,5] The effect of the perovskite deposition on the solar cells performance is critically important; it determines the film coverage, film thickness, film quality, and the transport properties.

[a]E-mail: lioz.etgar@mail.huji.ac.il

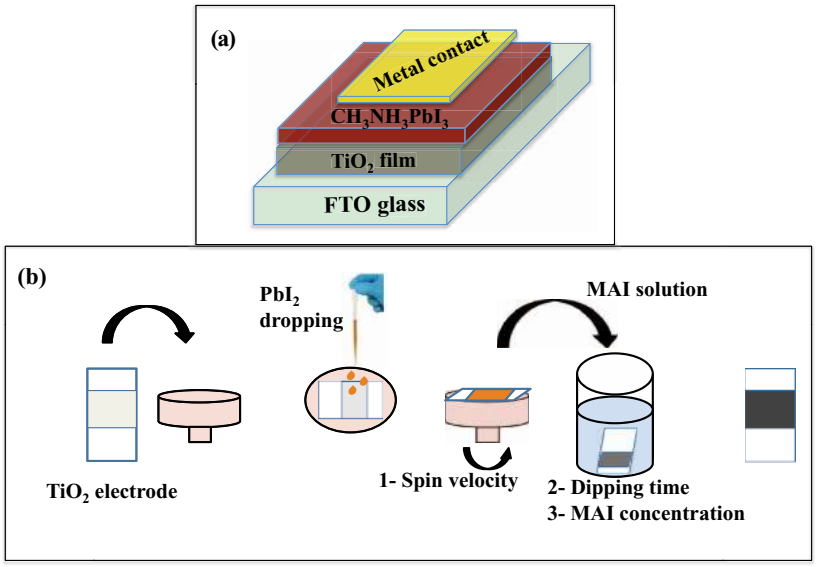

FIG. 1. (a) Schematic structure of the solar cell without a hole conductor; (b) the different stages involved in the two-step deposition of the $CH_3NH_3PbI_3$ perovskite. Methylammonium iodide (MAI) corresponds to CH_3NH_3I.

Graetzel and co-workers have demonstrated the use of the two-step deposition technique as a powerful technique for achieving highly efficient perovskite solar cells.[12] The two-step deposition enables better control over the perovskite crystallization by separating the perovskite deposition into the two precursors.

This paper describes an in-depth study of the parameters influencing the two-step deposition of perovskite in the solar cell. Hole conductor free perovskite solar cells were fabricated in this work, in order to minimize other possible effects. The influence of spin velocity, dipping time, annealing temperature, and methylammonium iodide (MAI) concentration on the photovoltaic (PV) performance are investigated. This study provides further understanding and control over the perovskite deposition through highly efficient perovskite-based solar cells.

This paper discusses the study of different parameters influencing the two-step deposition of $CH_3NH_3PbI_3$ perovskite in photovoltaic solar cells. The perovskite solar cell structure discussed is presented in Figure 1(a). $CH_3NH_3PbI_3$ functions both as a light harvester and hole transport material as discussed elsewhere.[15–18] This dual function simplifies the cell structure and minimizes the effect of other parameters that influence the PV performance, such as inconsistency in pore filling by the hole conductor.

Two-step deposition includes several stages: (a) dropping the PbI_2 solution onto the TiO_2 electrode; (b) spin coating the PbI_2 and heating the PbI_2; (c) dipping the PbI_2 electrode into CH_3NH_3I (CH_3NH_3I = MAI) solution; (d) annealing of the $CH_3NH_3PbI_3$ perovskite. Figure 1(b) shows the different stages in the deposition process. This paper describes changes in several important parameters in the deposition of the perovskite, showing the influence of these parameters on morphology, optical properties, and photovoltaic performance.

PbI_2 synthesis: The first step in the two-step deposition technique includes the PbI_2 precursor. Not much attention has been devoted to the synthesis of the PbI_2; usually this precursor is purchased from a supplier. In this study, the PbI_2 was synthesized in the lab according to reaction 1:

$$Pb(NO_3)_2 + 2KI \rightarrow PbI_2 + 2K^+ + 2NO_3^-. \quad (1)$$

The $Pb(NO_3)_2$ was reacted with potassium iodide (KI) at a ratio of 1:2 in water at 100 °C. The PbI_2 was precipitated immediately, filtered and dried in a vacuum oven. X-ray diffraction (XRD) analysis was performed on the synthesized PbI_2 and on PbI_2 purchased from Sigma-Aldrich. Figure 2 shows XRD of the lab-synthesized PbI_2 and of the purchased PbI_2. There is complete agreement between both spectra, indicating that the PbI_2 synthesized in the lab is the same as the standard

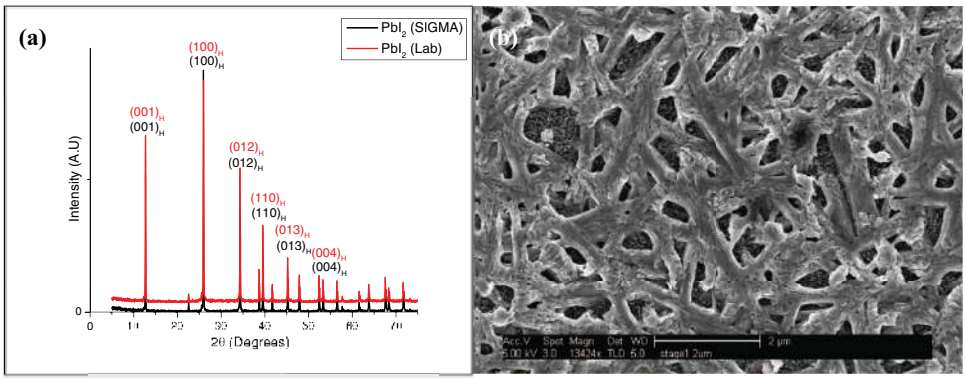

FIG. 2. (a) XRD spectra of the synthesized PbI_2 and PbI_2 purchased from Sigma-Aldrich. H corresponds to hexagonal. (b) HR-SEM micrograph of the synthesized PbI_2 deposited on mesoporous TiO_2.

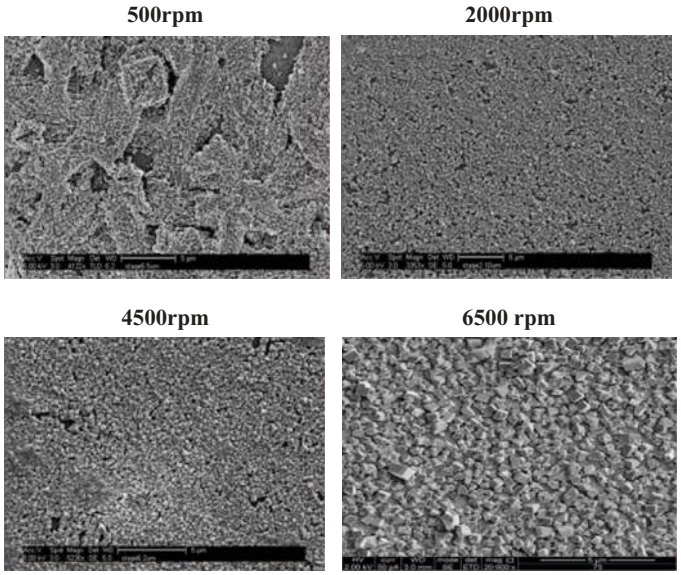

FIG. 3. Top view HR-SEM micrographs of $CH_3NH_3PbI_3$ crystals deposited on TiO_2 film at different spin velocities (rpm – rounds per minute).

purchased PbI_2. X-ray photoelectron spectroscopy (XPS) analysis also confirmed that there is no difference between the two versions of PbI_2. (For XPS spectra, please see Table S1 and Figure S1 in the supplementary material.)[19] Figure 2(b) presents high resolution scanning electron microscopy (HR-SEM) of the synthesized PbI_2 deposited on mesoporous TiO_2.

Spin velocity: The influence of spin velocity on PV performance was examined by changing the spin velocity of the PbI_2 on the TiO_2 film (process 1 in Figure 1(b)).

Figure 3 presents a top view HR-SEM of the $CH_3NH_3PbI_3$ at different spin velocities. The dipping time (related to process 2 in Figure 1(b), discussed in the section Dipping time) was the same for all spin velocities. It is seen that for 500 rpm the coverage of the $CH_3NH_3PbI_3$ is not complete; there are several voids. When the spin velocity is increased, the PbI_2 film is more uniform than when the spin velocity is low (low rpm) as seen at 2000 rpm, 4500 rpm, and 6500 rpm. The $CH_3NH_3PbI_3$ crystals increase in size with increased spin velocity. The reason for that is related to the dipping time in the CH_3NH_3I solution (process 2 in Figure 1(b)). As indicated in the previous paragraph, the dipping time in this set of experiments was the same – at 2000 rpm, the PbI_2 film is thicker than at 4500 rpm, while the thinnest PbI_2 film was observed at 6500 rpm. Different film thickness requires different dipping times. However, when the dipping time is the same, the resulting

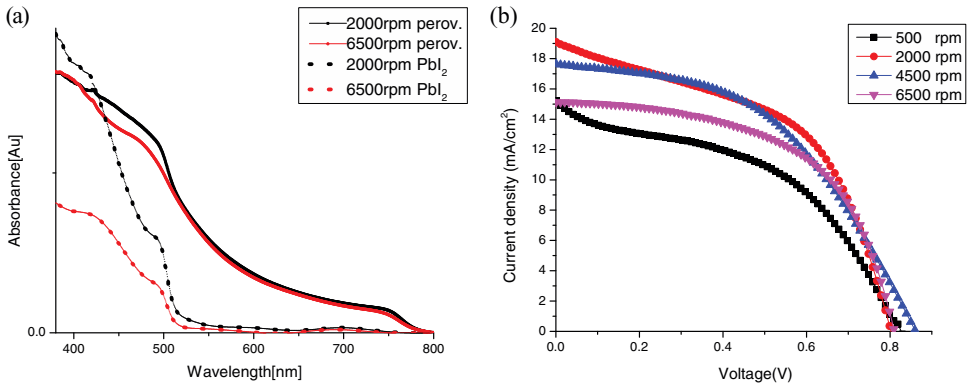

FIG. 4. (a) Absorbance spectra of different spin velocities for PbI_2 and $CH_3NH_3PbI_3$. (b) Current voltage curves of spin velocities cells.

TABLE I. PV parameters of the cells at different spin velocities.

Spin velocity (rpm)	v_{oc} (V)	J_{sc} (mA/cm^2)	FF (%)	Efficiency (%)
500	0.82	15.3	45	5.6
2000	0.80	19.1	51	7.8
4500	0.86	17.8	47	7.2
6500	0.81	15.2	56	6.9

crystals' size is dependent on the spin velocity (film thickness); therefore, in the case of 6500 rpm (the thinnest PbI_2 film thickness), the perovskite crystals were the biggest.

The difference in the film thickness of the PbI_2 and $CH_3NH_3PbI_3$ is supported by the absorbance spectra in Figure 4(a): two different spin velocities are presented, 2000 rpm and 6500 rpm. In the case of the absorbance of PbI_2, there is a big difference between the samples, related to thicker film of PbI_2 at 2000 rpm. In the case of the absorbance of $CH_3NH_3PbI_3$, the difference between the spin velocities can be observed, although it is lower than the difference between the PbI_2 samples. The explanation is related to the fact that the film thickness of the complete $CH_3NH_3PbI_3$ is also dependent on the dipping process of the PbI_2 electrode, which affected the final film thickness of the perovskite.

Table I and Figure 4(b) summarize the PV parameters and the current voltage curves (JV curves) of the cells at different spin velocities. The best PV results are achieved for the 2000 rpm sample with PCE of 7.8%. The data show that by changing the spin velocity, the current density of the solar cell is the parameter with the most influence.

Dipping time: The effect of dipping time in the CH_3NH_3I solution (process 2 in Figure 1(b)) on morphology and on PV performance was studied. Figure 5 presents dipping times of 20 s, 1 min, 20 min, and 3.5 h. It is noted that increasing the dipping time increases the size of the $CH_3NH_3PbI_3$ perovskite crystals (spin velocity was the same for all samples in these experiments), resulting in perovskite crystals the size of several micrometers.

The influence of dipping on PV performance is observed in Table II and Figure 6. The best PV performance was observed for the shortest dipping time of 20 s. Longer dipping time results in bigger crystals which affect transport through the perovskite film and enhance the recombination at longer dipping times, as indicated by the dark current measurements in Figure 6(a). The open circuit voltage (V_{OC}) and fill factors (FF) were lower for dipping times of 3.5 h and for 1 h, compared to the other dipping times.

Annealing temperature: The annealing step is the final stage before evaporation of the contact. (As indicated previously, no hole transport material is used in these cells.) To investigate the effect of the annealing temperature, several annealing temperatures were studied. Figure 7 presents HR-SEM micrographs of four annealing temperatures – 100 °C, 150 °C, 170 °C, and 200 °C. At

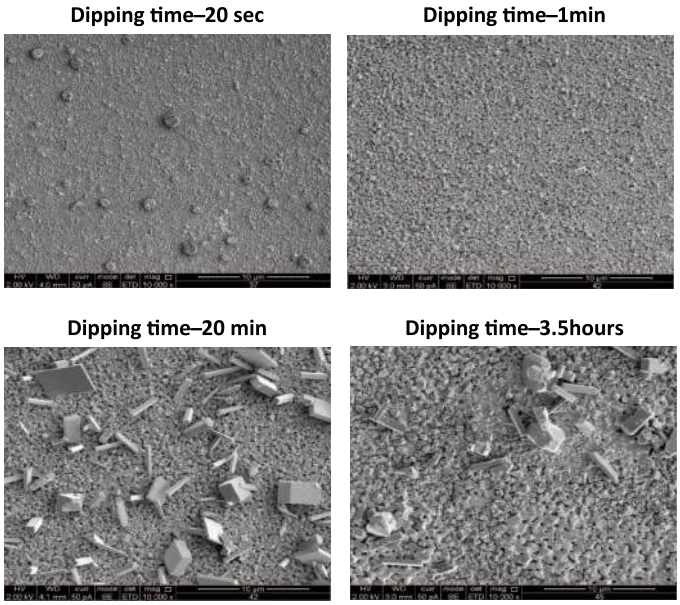

FIG. 5. Top view HR-SEM micrographs of $CH_3NH_3PbI_3$ crystals deposited on TiO_2 film at four different dipping times.

TABLE II. PV performance of the cells at 5 different dipping times.

Dipping time	V_{oc} (V)	J_{sc} (mA/cm^2)	FF (%)	Efficiency (%)
20 s	0.77	12.1	66	6.2
1 min	0.75	9.4	61	4.4
20 min	0.72	7.4	67	3.6
1 h	0.58	0.9	43	0.3
3.5 h	0.22	1.0	37	0.1

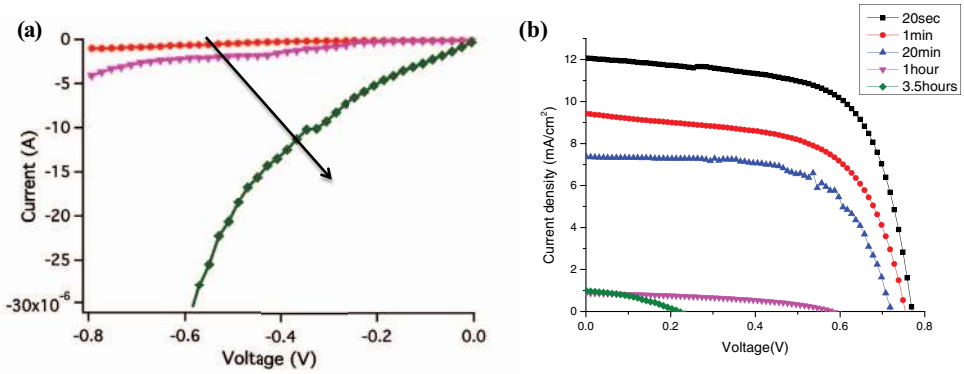

FIG. 6. (a) Dark current for various dipping times: 1 min, 1 h, 3.5 h. The arrow indicates the increase in the dark current. (b) Current voltage curves of the hole conductor free solar cells at different dipping times.

100 °C annealing temperature, the $CH_3NH_3PbI_3$ perovskite crystals are separate from each other. When increasing the annealing temperature to 150 °C, some of the perovskite crystals are sintered together, while at 170 °C annealing temperature, most of the perovskite crystals are sintered and there are no separate crystals of perovskite at the surface. At 200 °C annealing temperature, the $CH_3NH_3PbI_3$ perovskite crystals are melted, resulting in the lowest power conversion efficiency.

The PV performance and the current voltage curves of the different annealing temperatures are presented in Table III and Figure 8(b). The best photovoltaic performance was achieved at an

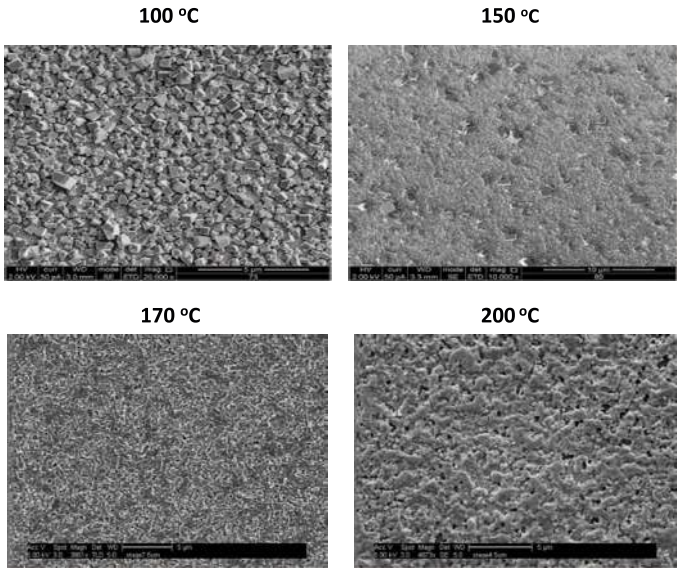

FIG. 7. Top view HR-SEM micrographs of $CH_3NH_3PbI_3$ crystals deposited on TiO_2 film and annealed at different temperatures.

TABLE III. PV results of different annealing temperatures.

Annealing Temperature (°C)	V_{oc} (V)	J_{sc} (mA/cm^2)	FF (%)	Efficiency (%)
70 °C	0.81	10.7	61	5.4
100 °C	0.86	14.5	55	6.8
150 °C	0.77	13.0	63	6.1
170 °C	0.80	17.7	62	8.7
200 °C	0.70	5.4	50	1.9

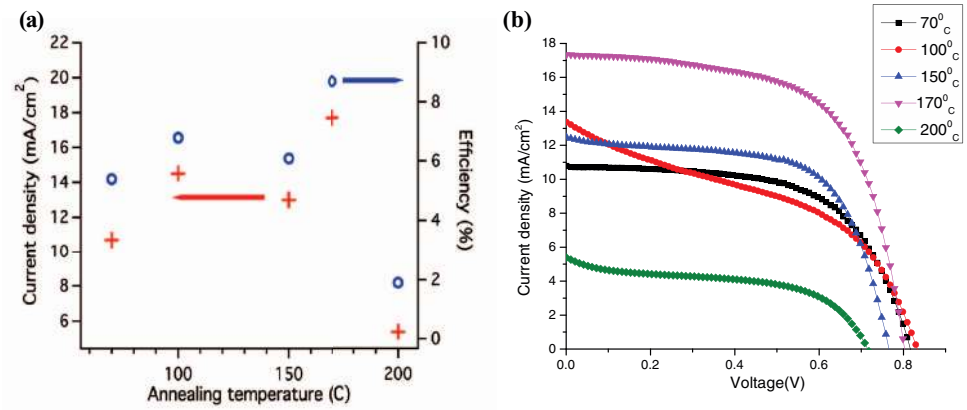

FIG. 8. (a) Current density and efficiency as a function of the annealing temperature. Current voltage curves of the hole conductor free perovskite solar cells annealed at different temperatures.

annealing temperature of 170 °C, and the highest current density was observed at this annealing temperature, probably a result of better sintering of the $CH_3NH_3PbI_3$ perovskite crystals than at the lower temperatures (70 °C, 100 °C, and 150 °C). Figure 8(a) summarizes the influence of the annealing temperature on the current density and the efficiency of the hole conductor free solar cells. Obviously, the annealing temperature mainly influences the current density.

Methylammonium iodide concentration: The concentration of MAI in the dipping solution has an important effect on the cells performance (process 3 in Figure 1(b)). Increasing the MAI

TABLE IV. PV parameters of cells made at different MAI concentrations in the dipping solution.

MAI concentration (M)	V_{oc} (V)	J_{sc} (mA/cm^2)	FF (%)	Efficiency (%)
0.06	0.80	19.1	51	7.8
0.09	0.77	18.9	65	9.4
0.12	0.84	16.9	47	6.6
0.15	0.8	10.9	58	4.8

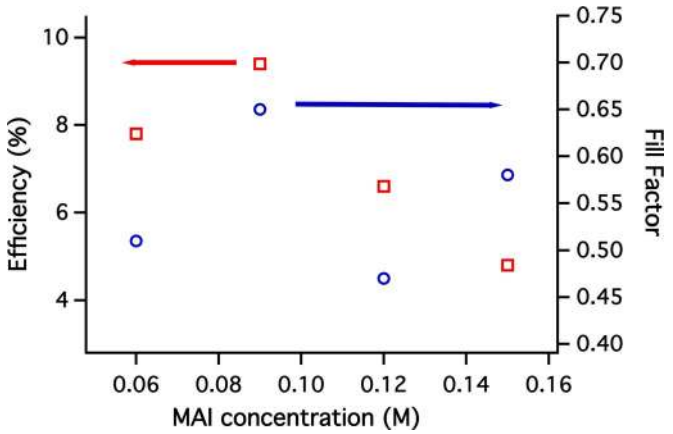

FIG. 9. Fill factor and efficiency of the hole conductor free perovskite solar cells at different MAI concentrations.

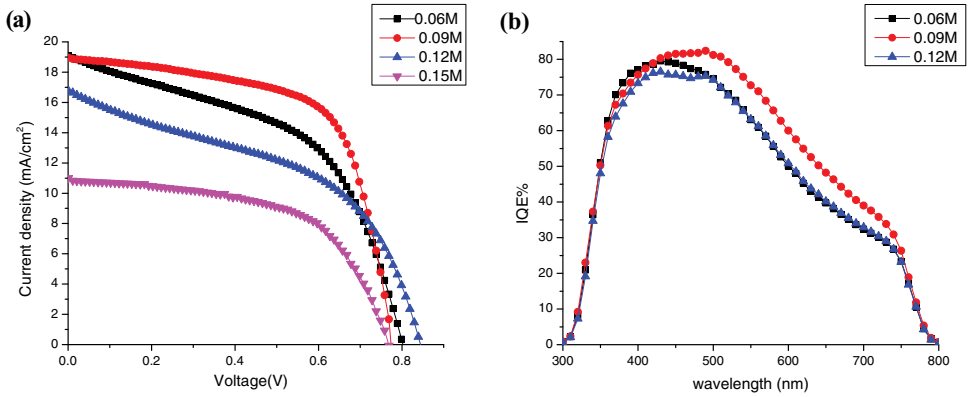

FIG. 10. (a) Current voltage curves of the different cells made at different MAI concentrations and the corresponding (b) IQE graphs.

concentration results in more MAI to react with the already deposited PbI_2, which could increase the crystallization of the $CH_3NH_3PbI_3$ perovskite. However, when an excess of MAI is present in the dipping solution, the free MAI (which did not react with the PbI_2) could have the opposite effect. The excess MAI might remain on the $CH_3NH_3PbI_3$ perovskite surface, reducing the perovskite conductivity. Moreover, excess MAI could cause desorption of the perovskite from the surface. Table IV shows the PV parameters at different MAI concentrations in the dipping solution. At high MAI concentration, the PV performance decreases due to a decrease in the current density. For low MAI concentration, the current density is high, although the FF is lower than the 0.09M MAI. Table IV shows that there is an optimum concentration where the FF and the current density are the highest, resulting in PCE of 9.4%, the highest efficiency in this study. Above this optimum point, both fill factor and efficiency decreased due to an excess of MAI in the dipping solution (Figure 9).

Current voltage curves and internal quantum efficiency (IQE) graphs are presented in Figures 10(a) and 10(b), respectively. IQE is the ratio of the number of charge carriers collected

by the solar cell to the number of photons of a given energy that is absorbed by the cell. The IQE spectra of the 0.09M MAI concentration achieved around 85% in the range of 400–550 nm.

In this research, the two-step deposition technique was used for the deposition of the $CH_3NH_3PbI_3$ in hole conductor free perovskite solar cells. The elimination of hole conductor in this study enabled isolating the effect of different parameters in the two-step deposition process and to investigate their influence on the PV performance. PbI_2 was synthesized in the lab avoiding contamination and non-desirable additives.

The effect on the photovoltaic performance was investigated by changing several parameters in the two-step deposition, i.e., spin velocity, dipping time, annealing temperature, and various methylammonium iodide concentrations. It was concluded that the spin velocity has the most influence on the J_{SC}, dipping time on the FF, annealing temperature on the J_{SC}, and MAI concentration on the FF and $J_{SC.}$ Interestingly, the V_{OC} was almost not affected by these parameters.

Understanding the effect of these critical parameters on perovskite deposition could lead to highly efficient, low-cost perovskite-based solar cells.

We would like to thank the Israel Alternative Energy Foundation (I-SAEF) that financed this research and to the Office of the Chief Scientist of the Ministry of Industry, Trade and Labor Kamin Project No.50303. We would like to thank Dr. Vladimir Uvarov from the Harvey M. Krueger Center for Nanoscience and Nanotechnology at the Hebrew University for the XRD measurements.

[1] N. G. Park, J. Phys. Chem. Lett. **4**, 2423–2429 (2013).
[2] H. J. Snaith, J. Phys. Chem. Lett. **4**, 3623–3630 (2013).
[3] A. Kojima, K. Teshima, Y. Shirai, and T. Miyasaka, J. Am. Chem. Soc. **131**, 6050–6051 (2009).
[4] H. S. Kim, C. R. Lee, J. H. Im, K. B. Lee, T. Moehl, A. Marchioro, S. J. Moon, R. Humphry-Baker, J. H. Yum, J. E. Moser, M. Gratzel, and N. G. Park, Sci. Rep. **2**, 591 (2012).
[5] See http://www.nrel.gov/ncpv/images/efficiency_chart.jpg for information about perovskite solar cells efficiency.
[6] N. J. Jeon, H. G. Lee, Y. C. Kim, J. Seo, J. H. Noh, J. Lee, and S. I. Seok, J. Am. Chem. Soc. **136**(22), 7837–7840 (2014).
[7] M. M. Lee, J. Teuscher, T. Miyasaka, T. N. Murakami, and H. J. Snaith, Science **338**, 643–647 (2012).
[8] S. D. Stranks, G. E. Eperon, G. Grancini, C. Menelaou, M. J. P. Alcocer, T. Leijtens, L. M. Herz, A. Petrozza, and H. J. Snaith, Science **342**, 341–344 (2013).
[9] G. C. Xing, N. Mathews, S. Y. Sun, S. S. Lim, Y. M. Lam, M. Gratzel, S. Mhaisalkar, and T. C. Sum, Science **342**, 344–347 (2013).
[10] D. Liu and L. Timothy, "Kelly, perovskite solar cells with a planar heterojunction structure prepared using room-temperature solution processing techniques," Nature Photonics **8**, 133–138 (2014).
[11] P. Docampo, J. M. Ball, M. Darwich, G. E. Eperon, and H. J. Snaith, "Efficient organometal trihalide perovskite planar-heterojunction solar cells on flexible polymer substrates," Nature Commun. **4**, 2761 (2013).
[12] Q. Chen, H. Zhou, Z. Hong, S. Luo, H.-S. Duan, H.-H. Wang, Y. Liu, G. Li, and Y. Yang, "Planar heterojunction perovskite solar cells via vapor-assisted solution process," J. Am. Chem. Soc. **136**, 622–625 (2014).
[13] M. Liul, M. B. Johnston, and H. J. Snaith, "Efficient planar heterojunction perovskite solar cells by vapour deposition," Nature (London) **501**, 395–399 (2013).
[14] J. Burschka, N. Pellet, S.-J. Moon, R. Humphry-Baker, P. Gao, M. K. Nazeeruddin, and M. Graetzel, Nature (London) **499**, 316 (2013).
[15] L. Etgar, P. Gao, Z. Xue, Q. Peng, A. K. Chandiran, B. Liu, Md. K. Nazeeruddin, and M. Grätzel, "Mesoscopic $CH_3NH_3PbI_3/TiO_2$ heterojunction solar cells," J. Am. Chem. Soc. **134**, 17396–17399 (2012).
[16] W. A. Laben and L. Etgar, "Depleted hole conductor-free lead halide iodide heterojunction solar cell," Energy Environ. Sci. **6**, 3249–3253 (2013).
[17] J. Shi, J. Dong, S. Lv, Y. Xu, L. Zhu, J. Xiao, X. Xu, H. Wu, D. Li, Y. Luo, and Q. Meng, Appl. Phys. Lett. **104**, 063901 (2014).
[18] S. Aharon, S. Gamliel, B. El Cohen, and L. Etgar, "Depletion region effect of highly efficient hole conductor free CH3NH3PbI3 perovskite solar cells," Phys. Chem. Chem. Phys. **16**, 10512–10518 (2014).
[19] See supplementary material at http://dx.doi.org/10.1063/1.4885548 for experimental details of the device fabrication, photovoltaic characterization, materials characterization, and XPS data of the PbI_2 synthesis.